REMLABNET - Solar system, new virtual laboratory with mathematical model using vector functions for primary, secondary and high schools and universities

Novel LDPE/vermiculite/ciclopiroxolamine hybrid nanocomposites: Structure, surface properties, and antifungal aktivity

Sylva Holešová[1], Karla Čech Barabaszová[1], Marianna Hundáková[1], Eva Plevová[2], Alena Kalendová[3]

[1]Nanotechnology Centre, VŠB - Technical University of Ostrava, Ostrava, Czech Republic

[2]Institute of Geonics, Academy of Sciences of Czech Republic (AS CR), Ostrava, Czech Republic
[3]Department of Polymer Engineering, Faculty of Technology, Tomas Bata University in Zlín, Zlín, Czech Republic

Correspondence: Sylva Holešová, Nanotechnology Centre, VŠB - Technical University of Ostrava, 17. listopadu 2172/15, 708 00 Ostrava -Poruba, Czech Republic. Email: sylva.holesova@vsb.cz

Abstract

The increasing number of indwelling medical materials and devices are connected with infections caused by yeast, especially Candida albicans. This pathogen produces biofilms on synthetic materials, which facilitates adhesion of the organisms to devices and renders them relatively refractory to medical therapy. Since antimicrobial polymer nanocomposites present one of the promising possibilities, this study explores a new approach to achieving this goal by developing nanocomposite based on low density polyethylene (LDPE) with clay mineral vermiculite as an active carrier for antifungal compound. The set of LDPE/clay nanocomposite with increasing amount of antifungal nanofiller was prepared by melt compounding procedure. As antifungal agent was selected generally used active substance ciclopiroxolamine and this compound was loaded into natural vermiculite through ultrasound technique. The structure of all prepared samples was studied by X-ray diffraction analysis and Fourier transforms infrared spectroscopy. Further thermal properties of poly-ethylene/clay nanocomposites were investigated by thermogravimetric analysis and the surface properties were evaluated by light optical microscopy, scanning electron microscopy and atomic force microscopy. From mentioned characteristics, we conclude that presence of nanofiller in LDPE primarily causes shift of thermal degradation to higher temperatures and increasing of microhardness. All prepared LDPE nanocomposites possess an excellent and prolonged antifungal activity against *Candida albicans.*

KEYWORDS: Drug delivery systems, clay, composites, structure-property relationships, thermogravimetric analysis (TGA)

1 INTRODUCTION

Among microbial infections, candidiasis becomes a growing problem and complication in many fields of medicine. The predominant agents for candidiasis include species of Candida, Aspergillus, and Cryptococcus when especially Candida albicans causes serious nosocomial infections, local or systemic life-threatening diseases and moreover possesses ability to form biofilms on variety of host tissues and surfaces, which are resistant against majority of known antifungal agents.[1-5] Some of the antifungal drugs have also limitation due to its low dissolution rate in the aqueous media resulting in low bioavailability. For that reason, the current topics of material research focus on development of antifungal materials with ability to inhibit growth of fungus and to develop a drug delivery system that can minimize side effects and increase drug bioavailability.[6-9]

Since polymers can act as matrix for holding the antimicrobial components and use of antimicrobial polymeric materials offers a guarantee of enhancing the efficiency of antimicrobial agents, polymeric nanocomposites and/or films are used in medicine for these unique proper-ties.[10,11] For several years, research into polymeric materials has also focused on the development of polymer/clay nanocomposites, as the resulting materials offer tremendous improvements in a wide range of physical and technical properties of low filler polymers.[12-15] Especially organoclay based polymer nanocomposites exhibit remarkable improvement in materials properties compared with virgin polymer or conventional micro and/or macro composites. Clay minerals are of particular interest because they can act as carriers of antimicrobial drugs for local treatment and thus to avoid treatment on the level of the entire organism in the first phase of the therapy.[16-19] There are several publications dealing with synthesis of polymer/organoclay nanocomposites and many of them focus on their antimicrobial properties.[17,20-24] The nanocomposites based on clay mineral montmorillonite are the most studied systems. However, only a tiny amount of these works deals with such polymer/organoclay nanocomposites that also exhibit specific antifungal behavior.[25-27] Zhou et al. prepared poly(dimethylsiloxane) (PDMS)/montmorillonite-terbinafine hydrochloride nanocomposite films with organoclay content <1 mass %, which strongly inhibited C. *albicans*.[25] Moreover these films showed excellent mechanical properties. Antimicrobial active films based on LDPE, ogano-modified mont-morillonite clay and carvacrol (used as essential oil model) were synthesized.[26] In this study the significant role of clay mineral was shown compared to films when polymer was compounded with pure carvacrol. Montmorillonite protected evaporation and degradation of highly volatile carvacrol during LDPE melt compounding resulting to higher content of carvacrol in final nanocomposite and also higher antimicrobial activity. These films were highly active against fungi Alternaria alternata. Rzayev et al. found that AgNPs had an important role in phase separation processing and formation of polymeric nanofibers with fine dispersed morphology and higher bioactive surface.[27] They prepared poly(vinyl alcohol-co-vinyl acetate)/ODA-MMT incorporated with in situ generated AgNPs by using electrospinning and centrifugal spinning techniques. These nanofibers showed high antifungal activity against Candida Spp fungals.

Polyethylene is one of the most used polymers globally, thanks to its cheap and easy production and moreover also represents a versatile biomaterial with many advantages, which is abundantly used in medicine as the basic material of various implants and devices.[28] Since one of the essential properties of these materials is anti-microbial/antifungal behavior we focused our work to preparation of new nanocomposite based on low-density polyethylene with antifungal properties. Our novel approach is to use the layered clay mineral vermiculite due to its greater layer charge than the most commonly used monmorillonite as an active carrier for antifungal compound ciclopirox olamine. Besides the antifungal activity against C. *albicans* we also investigated the structural, thermal and mechanical characteristics of prepared nanocomposites.

2 MATERIALS AND METHODS

2.1 Materials

Clay mineral vermiculite (abbreviated VER) from Letovice (Czech Republic) was milled in a planetary mill, sieved, and the fraction <40 μm was used for experiment. Its crystallochemical formula calculated from the results of the elemental chemical analysis was $(Si_{3.13}Al_{0.86}Ti_{0.02})(Mg_{2.53}Fe_{0.45}Al_{0.02})O_{10}(OH)_2(Mg_{0.19}K_{0.01}Ca_{0.02})$ per $O_{10}(OH)_2$ with the cation exchange capacity (CEC) 140 cmol(+)/kg. The CEC of VER was determined using repeated ion exchange with Cd(II) ions, then

saturated clay was separated by microfilter and washed out by deionized water. Ion exchanged Cd(II) was dissolved in HNO3 and determined by AES-ICP.[29] The chemicals used for the sample preparation were ciclopirox olamine (abbreviated CPA) and ethanol as a solvent. Powdered and granulated mixture of the industrial low-density polyethylene (abbreviated LDPE, Bralen RB 2-62L, SlovnaftCo., Slovak Republic) without additives was used as a starting material for preparation of polymer nanocomposite matrix.

2.2 Preparation of organovermiculite

Ethanolic solution of CPA was mixed with VER suspended in demineralized water in 1:1 weight ratio. The ultrasonic titanium sonotrode was placed to the dispersion in beaker and the mixture was subjected to ultrasound treatment with 505 amplitude for 60 min. After centrifugation, solid sample was dried at 75°C overnight and sample was named VER/CPA.

2.3 Preparation of LDPE nanocomposites

The set of LDPE_VER/CPA nanocomposites was prepared by melt-compounded procedure in mini compounder HAAKE MiniLab from mixture containing LDPE and nanofiller VER/CPA in weight ratios 1, 3, and 5 wt%. These mixtures were blended at 150° C for 15 min under 50 rpm velocity. Final samples were denoted as LDPE_1%VER/CPA, LDPE_3%VER/CPA, and LDPE_5% VER/CPA.

2.4 Samples characterization

The X-ray diffraction (XRD) patterns were measured using the X-ray diffractometer Rigaku Ultima IV (CuKα radiation, NiKβ filter, scintilation detector, Bragg-Brentano arrangement) in ambient atmosphere under constant conditions (40 kV, 40 mA, scanning range 1.5°-40° 2θ, scanning speed 1.925°/min). Figure of XRD patterns was drawn using the Origin9 software.

The IR spectra of powder samples were measured by potassium bromide pellets technique. Exactly 1.0 mg of sample was ground with 200 mg dried potassium bromide. This mixture was used to prepare the potassium bromide pellets. The IR spectra were collected using FT-IR spectrometer Nicolet iS50 (ThermoScientific) with DTGS detector. The measurement parameters were the following: spectral region 4000-400 cm^{-1}, spectral resolution 4 cm^{-1}; 64 scans; Happ-Genzel apodization. The IR spectra of LDPE nanocomposite samples were measured by ATR (Attenuated Total Reflectance) technique. The samples were lay and press by pressure device on the single-reflection diamond ATR crystal. The IR spectra were collected using FT-IR spectrometer Nicolet iS50 (ThermoScientific) with DTGS detector on Smart Orbit ATR accessory. The measurement parameters were as follows: spectral region 4000-400 cm^{-1}, spectral resolution 4 cm^{-1}; 64 scans; Happ-Genzel apodization.

Simultaneous thermogravimetry and differential thermal analysis were performed using the thermal analyzer Setsys 24 Evolution Setaram. The thermal curves were recorded under following conditions: argon atmosphere (10 ml min^{-1}), final temperature 800° C, heating rate 10° C min^{-1} and sample mass about 10 mg. The parameters such as final weight loss (Δm), the onset temperatures and the temperature of maximum weight loss T_{max} were determined from thermal curves.

Surface morphology of LDPE nanocomposite plates was investigated using scanning electron microscope (SEM) QUANTA 450 SEG, FEI. The SEM images were obtained in the low vacuum and using

a secondary electron detector (SE) operated at 20 kV. Prior to characterization, the samples were coated with a gold thin film to avoid electrical charging during the observation.

The VER/CPA nanofiller arrangements in LDPE matrix were analyzed with 3D optical light microscope (LM) VHX-2000 (Keyence Corporation, Japan) at the plate area of 3 X 3 mm.

The topography and roughness of the surfaces of LDPE nanocomposite plates were studied using Solver NEXT (NT-MDT) atomic force microscope (AFM). Noncontact mode with 8 μm z-linearized dry scanner with a silicon probe 1650-00 was employed for AFM scanning. The images and roughness dates were evaluated using Gwyddion 2.28 software at the LDPE plate area of 25 X 25 µm.

The role of VER/CPA nanofillers on mechanical properties of LDPE nanocomposite plates was evaluated by the microhardness in different places in the range 100-100 µm polymer plates and was measured by Vickers microhardness tester (Micro Combi Tester, MHT3, Anton Paar). The indenter was a square shaped diamond pyramid with top angle of 136°. In this study, the microhardness tests were performed under the applied load of 500 mN and the loading time was 90 s. The result values are average results of 10 imprints. Instrumentation hardness testing was according to CSN EN ISO 14577.

2.5 Antifungal tests

2.5.1 Antifungal test of Organovermiculite

The minimum inhibitory concentration (MIC) of the prepared powder organovermiculite sample VER/CPA was determined by its lowest concentration that would completely inhibit fungi growth. The dilution and cultivation were performed on 96-well microtitration plates. The highest applied concentration was 10% (w/v) over water dispersion. This dispersion was further diluted by a threefold diluting method in glucose stock in such a manner that the second to seventh set of hollows contained sample dispersed in concentrations of 3.33%, 1.11%, 0.37%, 0.12%, 0.04%, and 0.01%. The eighth set of wells contained pure glucose stock as a control test. The volume of 1 **p**l of glucose suspension of C. albicans ATC90028 (1.1 X 109 cfu ml^{-1}), provided by the Czech collection of microorganisms (CCM), was applied into the hollows. The volume of 1 **p**l of yeast suspensions was transferred (after 30, 60, 90, 120, 180, 240, and 300 min and then in 24 h intervals for 5 days) from each well into 100 pl of the fresh glucose stock and incubated in a thermostat at 37° C for 24 and 48 h. Antifungal activity was evaluated by turbidity, which is a display of bacterial growth.[30]

2.5.2 Antifungal test of LDPE Nanocomposites

Antifungal test of all prepared LDPE nanocomposites was performed by microbial fingerprints technique. This method of direct fingerprints assumes that the microbe under the same conditions gradually dies. Each sample plate was cut to the three squared plates (25 cm^2). The volume of 25 μl of glucose suspensions of Candida albicans ATC 90028 (1.0 x 10^5cfu ml^{-1}), provided by the Czech collection of microorganisms (CCM), were spread on the plates and were left to dry in the laminar box at 21°C. Then the dried yeast suspension on the surface of plates was stamping using microbial fingerprints technique on the three discs with Sabouraud agar in 24, 48, 72, and 96 h time intervals. The yeast cultivation took place in thermostat at 30° C for 48 h. The number of colony-forming units of bacteria (CFU) at all three fingerprints were counted next day and averaged.

3 RESULTS AND DISCUSSION

3.1 X-Ray diffraction

The XRD pattern of the initial VER shows the sequence of the basal reflections (**Figure 1**). The value *d* (002) = 1.436 nm which is characteristic for VER structure, confirm the presence of two layers of water molecules around the exchangeable cations in the VER interlayer space. The basal reflections are rapidly changed in VER/CPA sample. The XRD pattern of VER/CPA shows new reflections with d-values 1.577, 1.309, 0.455, and 0.318 nm that confirms the intercalation of CPA in the interlayer space of VER as result of displacement of water molecules and hydrated interlayer cations. However, due to d-values, the CPA molecules are variously arrangements in the interlayer space of VER.

The XRD pattern of original LDPE (**Figure 1**) shows the reflections of crystalline region with d = 0.415 nm and d = 0.375 nm and region of the amorphous phase between 15° and 25° 2θ.[31] After incorporation of VER/-CPA into LDPE matrix, basal reflection was shifted from d = 1.309 nm to d = 1.284 nm (LDPE_1%VER/CPA), *d* = 1.275 nm ((LDPE_3%VER/CPA) and d = 1.276 nm ((LDPE_5%VER/CPA) probably due to rearrangement of interlayer material. Reflections of LDPE are without significant change of crystalline region. Relative intensity of reflections depends on amount of VER/CPA nanofiller.

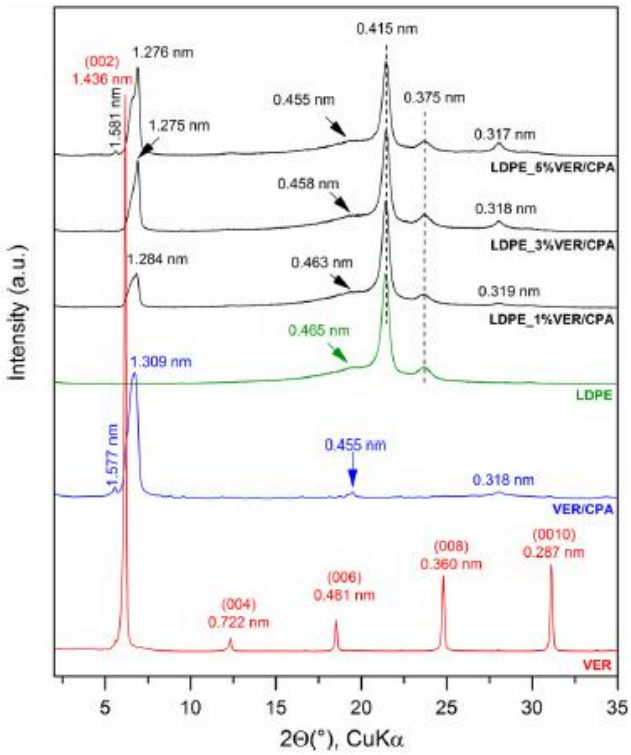

FIGURE 1 XRD patterns of initial VER, VER/CPA, original LDPE and LDPE_VER/CPA nanocomposites [Color figure can be viewed at wileyonlinelibrary.com]

3.2 FTIR spectroscopy

The FTIR spectrum of initial natural VER **(Figure 2**a) shows a band at 3674 cm^{-1} in O-H stretching region attributed to Mg_3OH unit and, together with absorption at 668 cm^{-1} belonging to O—H bending vibration, these bands suggest trioctahedral character of this VER.[32] Absorption at 3566 cm^{-1} in O—H stretching region belongs to Fe_2OH unit. The presence of this band indicates that although this vermiculite is nominally trioctahedral, some of the OH groups are associated with vacancies and are in local dioctahedral environment.[32] Absorption observed at 3368 cm^{-1} corresponds to O—H stretching vibration of adsorbed water and those at 1653 cm^{-1} to O-H bending vibration of adsorbed water.

Finally, an intensive band at 1001 cm^{-1} was assigned to Si—O stretching vibration together with Si—O bending vibration at 446 cm^{-1}.[32] The FTIR spectrum of CPA (**Figure 2**b) shows characteristics bands at 3136, 3057, 2925, 2853, and 2749 cm^{-1} corresponded to the O—H stretching vibration, aromatic C—H stretching vibrations, asymmetric and symmetric CH_2 stretching vibrations, deformation overtone of CH_3, respectively.33,34 Absorptions at 1639, 1541, and 1511 cm^{-1} belong to Amide I and Amide II band (C=O stretching and N—H deformation vibrations).

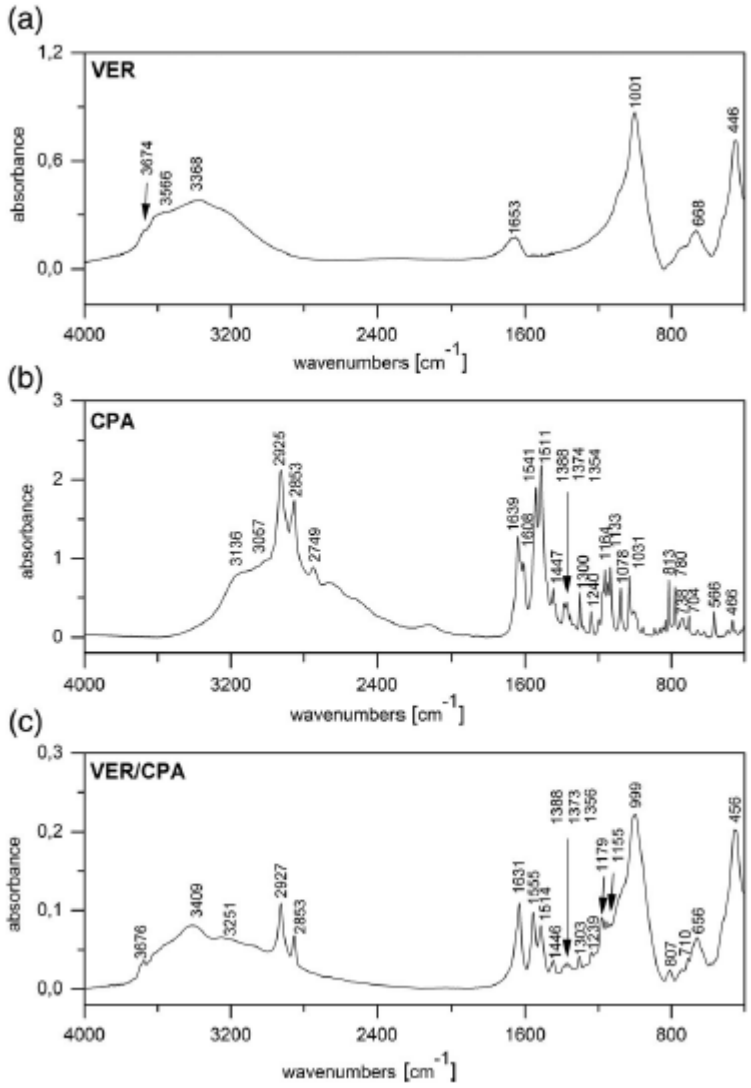

FIGURE 2 FTIR spectra of (a) initial VER, (b) CPA, and (c) VER/CPA

The bands that occurred in the 1447-1354 cm-interval are due to the C—H deformation vibrations of CH_2 and CH_3 groups as well as in 1174-1133 cm^{-1} interval.33,34 In the spectrum of nanocomposite VER/CPA (**Figure 2**c) we can observe shift (3409 cm^{-1}) and enlargement in the region of characteristic stretching vibrations of O-H groups originate from VER. This situation suggests creation of hydrogen bond between OH groups from VER and OH group from CPA, which are in connection with amide group. This phenomenon also involves a shift in the area corresponding to the Amide II bands (1555 cm^{-1}).

The FTIR spectrum of the original LDPE (**Figure 3**) shows main bands at 2915, 2848, 1471, and 718 cm^{-1}. These bands are due to the asymmetric and symmetric C—H stretching, deformation and rocking

vibrations. If the polymer has significant branching, the additional weak band at 1377 cm^{-1} is observed.[34] Except characteristic vibrations of pure LDPE the FTIR spectra of LDPE_VER/CPA nanocomposites (**Figure 3**) shows bands corresponded to the Si—O stretching and bending vibrations. The intensity of these bands increased with increasing amount of nanofiller.

3.3 Thermogravimetric analysis

The **Figure 4** shows TG and DTG curves of original LDPE and LDPE nanocomposites. The mass loss is determined in the temperature interval 300-700° C (Figure 4a). The highest mass loss 99.1% is obtained for sample of original LDPE and the lowest mass loss 94.1% for a nanocomposite sample with the highest amount of nanofiller (LDPE_5% VER/CPA) (**Table 1**). According to DTG curves, the mass loss in the temperature interval 300-700°C is realized for all samples at one step (**Figure 4**b). These results are in agreement with literature, which reports that polyethylene decomposes into a large number of paraffinic and olefinic compounds without a residue.[35] The lowest temperature of maximum reaction velocity T_{max} is found for sample LDPE, the highest value of T_{max} was obtained for sample LDPE_5%VER/CPA (**Table 1**).

It is important to note that the starting temperature of degradation (T_d) is higher for all LDPE nanocomposites in contrast to the original LDPE (**Table 1**), which means that the addition of VER/CPA nanofiller causes the increasing of thermal stability of LDPE.

3.4 LDPE surface morphology, topography, and microhardness

The LM images of LDPE nanocomposites plates (Figure 5a) reveal the distribution of VER/CPA in LDPE matrix. The original LDPE plate is completely transparent, not cloudy and without surface defects and cavities. As we can observe, the VER/CPA nanofillers are in the samples LDPE_1%VER/CPA and LDPE_3%VER/CPA very well dispersed in LDPE matrix and individual nanoparticles are separated from each other. The increasing VER/CPA filler content results in the LDPE plates becoming cloudy, moreover LDPE_5%VER/CPA plates become light brown in color, nevertheless the LDPE plates still remains transparent. The VER/CPA nanofiller particles in LDPE_5%VER/CPA are dispersed more nonuniformly, created the larger particles about 40 μm in diameter. It can be assumed that part of VER/CPA nanofiller particles experienced a coalescence phenomenon, so that it could not be dispersed well in the polymer matrix. The agglomeration behavior was not observed.

The surface morphology of LDPE plates was observed using SEM microscope and is presented in Figure 5b). The LDPE plate is clear and transparent with a homogenous and smooth surface morphology. Sporadically, theholes are evident on the original LDPE surface with a diameter around 1 μm and object which should be caused by powdering of plates by gold powder before SEM measurement.

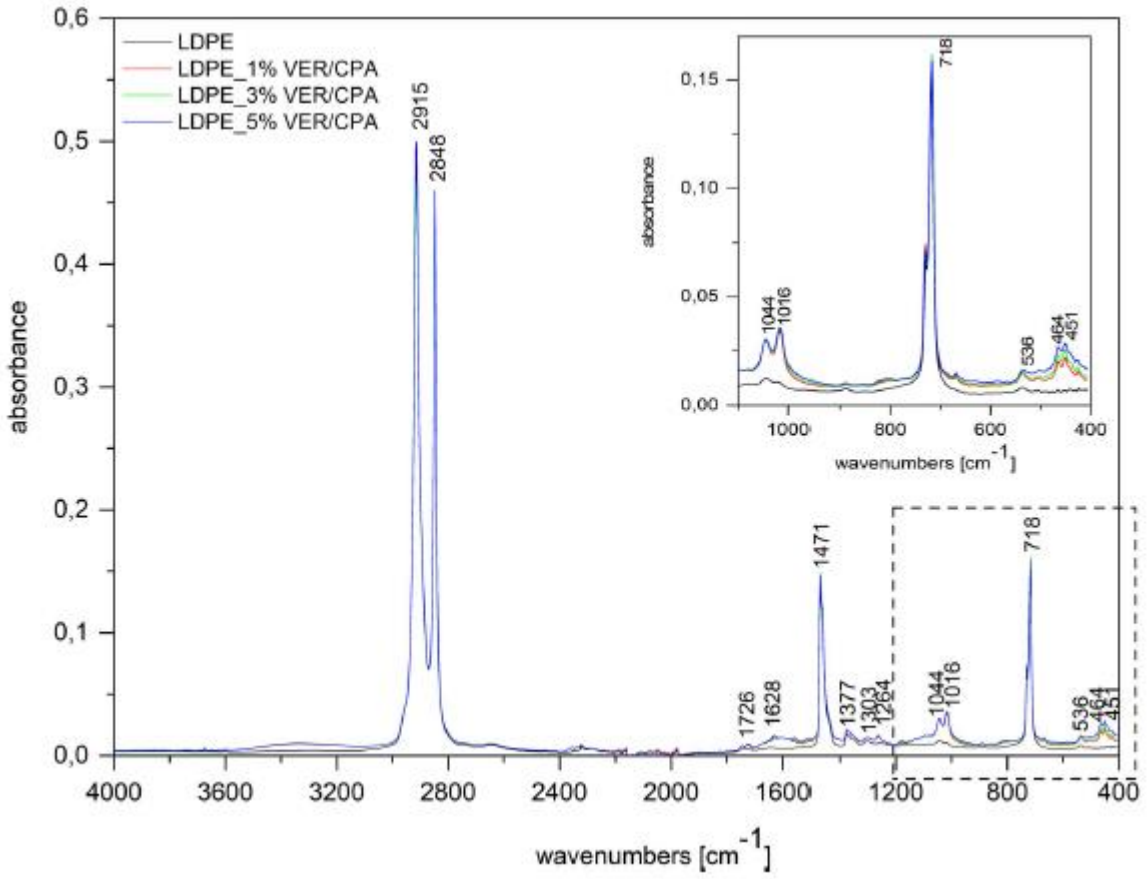

FIGURE 3 FTIR spectra of original LDPE and LDPE_VER/ CPA nanocomposites with zoomed region 1200-400 cm^{-1} [Color figure can be viewed at wileyonlinelibrary.com]

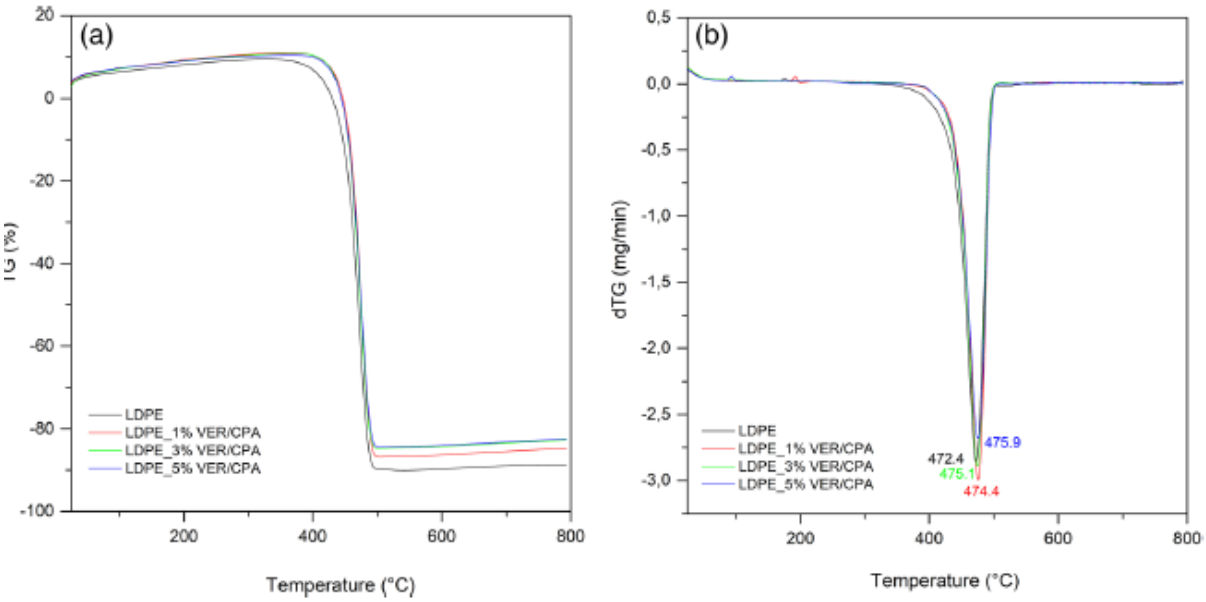

FIGURE 4 (a) TG and (b) DTG curves of original LDPE and LDPE_VER/CPA nanocomposites [Color figure can be viewed at wileyonlinelibrary.com]

TABLE 1 Thermal data of original LDPE and LDPE nanocomposites obtained from TG and DTG curves

Sample	Δm (%)	T_d (°C)	T_{max} (°C)
LDPE	99.1	434.1	472.4
LDPE_1%VER/CPA	96.9	444.5	474.4
LDPE_3%VER/CPA	94.5	442.2	475.1
LDPE_5%VER/CPA	94.1	441.0	475.9

LDPE_VER/CPA nanocomposite plates have relatively smoothed surface with visible gentle and unidirectionally oriented wrinkles. From SEM images, it is evident that the VER/CPA nanofiller is homogenously and well dispersed in the matrix, mostly in the direction perpendicular to the surface plate LDPE.

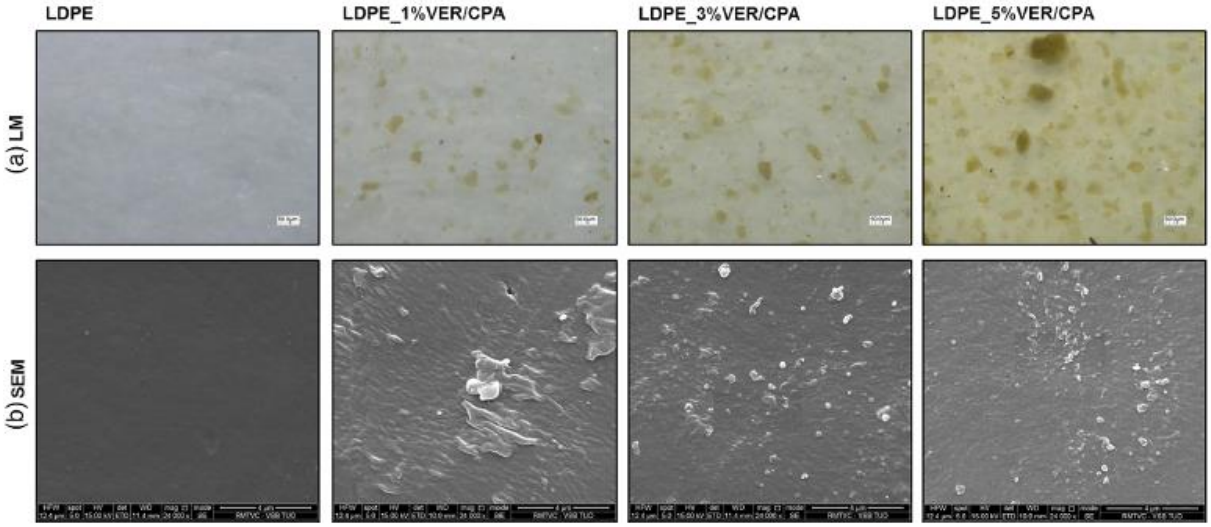

FIGURE 5 The LM (a) and SEM (b) images of the original LDPE and LDPE nanocomposites surface [Color figure can be viewed at wileyonlinelibrary.com]

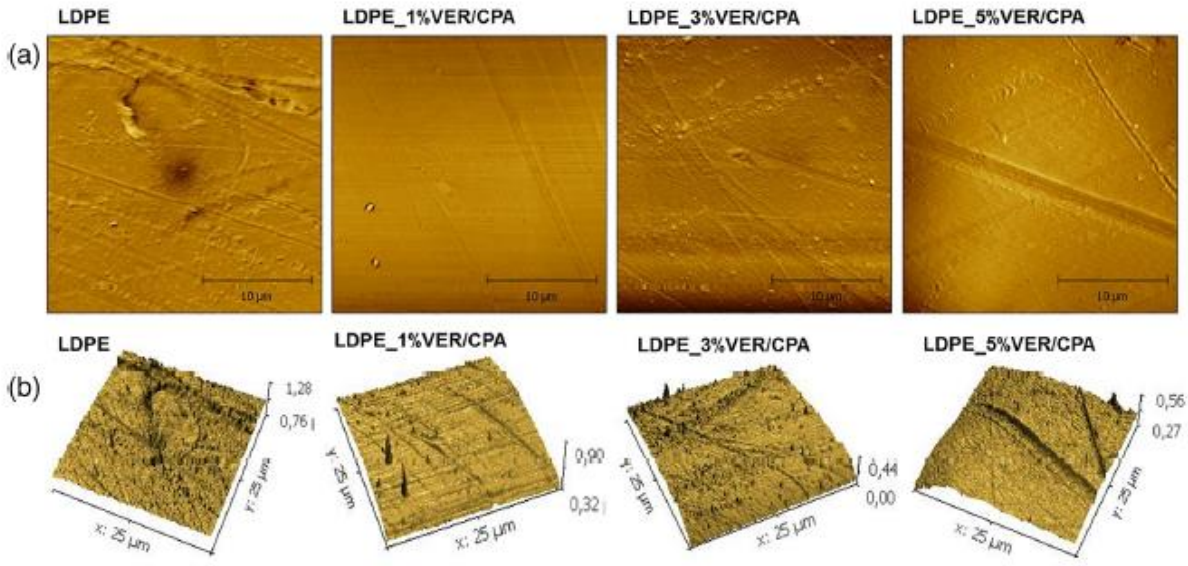

FIGURE 6 AFM surface topography: (a) 2D and (b) 3D images of the original LDPE and LDPE nanocomposites plates [Color figure can be viewed at wileyonlinelibrary.com]

In some places, the bigger fractions of VER/CPA nanofillers are incorporated in the horizontal direction (best visible in the LDPE_1%VER/CPA sample, Figure 5b) to the LDPE plates surface. No surface defects are detected in their region. This homogeneous dispersion and strong adhesion could be due to the good compatibility between LDPE and nanoparticles of the VER/CPA nanofillers.

For more detailed surface study, the contact modes of AFM measurement were used to observe surface topography of the LDPE plates at the room temperature. For AFM scanning identical samples were used as for SEM scanning. Typical surface in the 2D and 3D images are shown in the **Figure 6**. The surface roughness of the LDPE samples is evaluated from the line analyses realized outside the surface defect/grooves (average values of eight measurements, Ra). The measured values are summarized in **Table 2**.

As we can observe from the AFM images (**Figure 6**), all LDPE nanocomposite plates exhibit a relatively low roughness in the range of 11.5-18.8 nm (**Table 2**). The LDPE_5% VER/CPA plate (with the highest nanofiller content) possesses the highest roughness (18.8 nm).

TABLE 2 The average values of the surface roughness (Ra, line analysis) of the original LDPE and LDPE nanocomposites surfaces—AFM measurements

Sample	Ra (mm)	HIT (MPa)	HV (−)	hm (μm)
LDPE	12.6 (0.8)	20.9 (1.6)	2.0 (0.2)	37.4 (1.8)
LDPE_1%VER/CPA	11.5 (1.7)	23.1 (0.7)	2.2 (0.1)	34.8 (0.4)
LDPE_3%VER/CPA	13.3 (2.2)	22.5 (1.0)	2.1 (0.1)	35.5 (0.8)
LDPE_5%VER/CPA	18.8 (3.6)	25.7 (1.7)	2.4 (0.2)	32.6 (0.9)

Note: Standard deviations are provided in parentheses.

Abbreviations: HIT, indentation hardness; HV, Vickers microhardness; hm, maximum impression depth.

TABLE 3 MIC values (%) (w/v) of VER/CPA

		MIC (% w/v)											
Strain	Sample	30 Min	60 Min	90 Min	120 Min	180 Min	240 Min	300 Min	1 Day	2 Days	3 Days	4 Days	5 Days
Candida albicans	VER/CPA	10	10	10	10	10	3.33	3.33	0.12	0.12	0.014	0.014	0.014

TABLE 4 Average numbers of fungal colony-forming units (CFU) of used strains at the various time intervals for LDPE nanocomposites

		Number of CFU Time of contact [h]			
Strain	Sample	24	48	72	96
Candida albicans	LDPE_1%VER/CPA	119	37	38	0
	LDPE_3%VER/CPA	163	15	30	1
	LDPE_5%VER/CPA	256	5	0	0

The bigger defects are evident in 2D images of original LDPE and LDPE_3%VER/CPA plates, which are mainly due to the presence of fine grooves formed during the processing of the LDPE plates. Maximal peaks correspond to the presence of gold powder used before SEM measurement are evident in all AFM images. These could slightly affect the resulting numerical roughness values. The surface roughness of the LDPE_1%VER/CPA plate is generally the lowest.

The mechanical properties as indentation hardness (HIT), Vickers microhardness (HV), and maximum impression depth achieved (hm) are measured and the result are summarized in **Table 2**. For a purpose to provide reliable microhardness values corresponding to the total hardness of the nanocomposites, the imprints under each load should be larger in size than the dimensions of the dispersed VER/CPA nanofillers (around 10 μm). It is known that the mean diagonal length of the imprints varies in the range of 100-200 μm. The measured values in maximum impression depth (hm) range from 32.6 to 37.4 μm. This means that the imprints are always larger than the dimensions of the dispersed VER/CPA nanofillers and their depth decreases with the increasing content of VER/CPA nanofillers in the LDPE matrix. These measurements correlate with HIT results where the HIT value increases from 20.9 MPa (LDPE) to 25.7 MPa (LDPE_5% VER/CPA) with increasing amount of nanofiller. These values correlate with the Vickers microhardness values, where 2.0 HV is for original LDPE and increases to 2.4 HV for LDPE_5%VER/CPA.

4 ANTIFUNGAL TESTS

4.1 Antifungal test of organovermiculite

Antifungal test of nanofiller VER/CPA was performed against yeast C. albicans and the activity expressed by minimum inhibitory concentrations (MIC) is shown in **Table 3**. We obtained significant results (the lowest MIC value 0.014 [% w/v] after 3 days) in longer time intervals opposite to antifungal activity in short time intervals, which is poor.

4.2 Antifungal test of LDPE nanocomposites

Antifungal activity of prepared LDPE nanocomposites was studied using microbial fingerprints technique. Twenty-five microliters of microbial suspension with density 10^5 CFU/ml were spread on 2.5 cm^2 surfaces of tested squared plates of LDPE nanocomposites, which mean that the original density of suspension on squared plates dropped one logarithmic order. Average numbers of fungal colony-forming units (CFU) at various time intervals are shown in **Table 4**. We obtained very good results in longer time intervals, when from 48 to 96 h only minimum of CFU survives, moreover after 72 h the sample with the highest amount of nanofiller (sample LDPE_5%VER/CPA) causes total extermination of C. albicans. These samples possess significant levurocidal efficiency.

5 CONCLUSION

In this work, LDPE nanocomposites with antifungal nanofiller based on vermiculite and ciclopirox olamine were prepared by melt compounding method. The XRD and FTIR analyses confirmed successful intercalation of antifungal compound ciclopirox olamine into structure of natural clay vermiculite and also presence of thus prepared nanofiller in LDPE polymeric matrix. Thermal analysis proved that the addition of VER/CPA nanofiller causes the increasing of thermal stability of LDPE. The images from LM and SEM show that lower amount of nanofiller VER/CPA (1 and 3 wt%) is very well

dispersed in LDPE matrix, while higher amount of VER/CPA (5 wt %) already causes nonuniform dispersion and creation of bigger particles in matrix. As we observed from the AFM images, all LDPE nanocomposites exhibited a relatively low roughness, which increased with increasing amount of nanofiller VER/CPA. As well results from indentation hardness tests confirmed increasing microhardness with increasing amount of nanofiller in LDPE matrix. Finally, all prepared LDPE nanocomposites exhibited strong antifungal activity against C. albicans predominantly at longer time intervals. Thus, these new nanocomposites have a high potential for antifungal medical materials application due to their long-lasting antifungal efficacy.

REFERENCES

[1] M. A. Pfaller, D. J. Diekema, Clin. Microbiol. Rev. 2007, 20, 133.

[2] C. G. Pierce, T. Vila, J. A. Romo, D. Montelongo-Jauregui, G. Wall, A. Ramasubramanian, J. L. Lopez-Ribot, J. Fungi 2017, 3,1.

[3] G. Wall, D. Montelongo-Jauregui, B. Vidal Bonifacio, J. L. Lopez-Ribot, P. Uppuluri, Curr. Opin. Microbiol. 2019, 52, 1.

[4] G. Morace, F. Perdoni, E. Borghi, J. Glob. Antimicrob. Re. 2014, 2, 254.

[5] N. M. Revie, K. R. Iyer, N. Robbins, L. E. Cowen, Curr. Opin. Microbiol. 2018, 45, 70.

[6] S. H. S. Dananjaya, R. Saravana Kumar, M. Yang, C. Nikapitiya, J. Lee, M. De Zoysa, Int. J. Biol. Macromol. 2018, 108, 1281.

[7] M. Ghosh, S. Mandal, A. Roy, S. Chakrabarty, G. Chakrabarti, S. Kumar Pradhan, Mater. Sci. Eng. C 2020,106, 110160.

[8] C. Li, X. Wang, F. Chen, C. Zhang, X. Zhi, K. Wang, D. Cui, Biomaterials 2013, 34, 3882.

[9] C. Vilela, H. Oliveira, A. Almeida, A. J. D. Silvestre, S. C. R. Freire, Carbohydr. Polym. 2019, 217, 207.

[10] A. Mufloz-Bonilla, M. Fernandez-Garcia, Prog. Polym. Sci. 2012, 37, 281.

[11] E. R. Kenawy, S. D. Worley, R. Broughton, Biomacromolecules 2007, 8, 1359.

[12] S. Pavlidou, C. S. Papaspyrides, Prog. Polym. Sci. 2008, 33,1119.

[13] M. Kotal, A. K. Bhowmick, Prog. Polym. Sci. 2015, 51, 127.

[14] P. Kiliaris, C. D. Papaspyrides, Prog. Polym. Sci. 2010, 35, 902.

[15] E. I. Unuabonah, A. Taubert, Appl. Clay Sci. 2014, 99, 83.

[16] G. Ozdemir, S. Yapar, M. Ho§gor Limoncu, Appl. Clay Sci. 2013, 72, 201.

[17] N. Meng, N. L. Zhou, S. Q. Zhang, J. Shen, Appl. Clay Sci. 2009, 42, 667.

[18] S. Holešová, M. Valášková, E. Plevová, E. Pazdziora, K. Matějová, J. Colloid Interface Sci. 2010, 342, 593.

[19] S. Holešová, J. Štembírek, L. Bartošová, G. Pražanová, M. Valášková, M. Samlíková, E. Pazdziora, Mater. Sci. Eng. C 2014,42, 466.

[20] S. Holešová, M. Reli, M. Hundáková, K. Čech Barabaszová, M. Ritz, E. Plevová, E. Pazdziora, J. Nanosci. Nanotechnol. 2019, 19, 2925.

[21] R. Nigmatullin, F. Gao, V. Konovalova, J. Mater. Sci. 2008, 43, 5728.

[22] S. M. Meister Meira, G. Zehetmeyer, A. Izé Jardim, J. M. Scheibel, R. Vinicius Bof de Oliveira, A. Brandelli, Food Bio-proc. Technol. 2014, 7, 3349.

[23] N. Fong, A. Simmons, L. A. Poole-Warren, Acta Biomater. 2010, 6, 2554.

[24] M. C. Wang, J. J. Lin, H. J. Tseng, S. H. Hsu, ACS Appl. Mater. Interfaces 2012, 4, 1338.

[25] N. Meng, N. L. Zhou, S. Q. Zhang, J. Shen, Appl. Clay Sci. 2009, 46, 136.

[26] R. Shemesh, M. Krepker, D. Goldman, Y. Danin-Poleg, Y. Kashi, N. Nitzan, A. Vaxman, E. Segal, Polym. Adv. Technol. 2015, 26, 110.

[27] Z. M. O. Rzayev, D. Erdonmez, K. Erkan, M. Sim§ek, U. Bunyatova, Int. J. Polym. Mater. PO 2015, 64, 267.

[28] N. C. Paxtona, M. C. Allenby, P. M. Lewis, M. A. Woodruff, Eur. Polym. J. 2019,118, 412.

[29] Z. Klika, J. Seidlerová, M. Valášková, C. Kliková, I. Kolomazník, Appl. Clay Sci. 2016,132-133, 41.

[30] J. Kneiflová, Česk. Epidemiol. Mikrobiol. Imunol. 1988, 37, 97.

[31] D. K. Das-Gupta, IEEE Electr. Insul. Mag. 1994,10, 5.

[32] V. C. Farmer, in The Infrared Spectra of Minerals (Ed: V. C. Farmer), The Mineralogical Society, London, UK 1974.

[33] R. M. Silverstein, G. C. Basser, T. C. Morrill, Spectrometric Identification of Organic Compounds, 2nd ed., John Wiley & Sons Inc., New York, NY 1991.

[34] G. Socrates, Infrared and Raman Characteristic Group Frequencies, Tables and Charts, 3rd ed., John Wiley & Sons Inc., Chichester, UK 2001.

[35] H. Bockhorn, A. Hornung, U. Hornung, D. Schawaller, J. Anal. Appl. Pyrol. 1999, 48, 93.